



READ 2024
RESEARCH & EDUCATION IN AIRCRAFT DESIGN
WARSAW, POLAND | 6-8 NOVEMBER 2024



INTEGRATED AUTOMATIC CONTROL OF THE ARCHER COMPOUND HELICOPTER

Sebastian Topczewski¹, Sara Waśniewska² & Tomasz Cioć³

¹Division of Automation and Aeronautical System, Institute of Aeronautics and Applied Mechanics, Faculty of Power and Aeronautical Engineering, Warsaw University of Technology

²Faculty of Power and Aeronautical Engineering, Warsaw University of Technology

³Enter Air

Abstract

This paper presents the results of studies on automatic flight control systems for helicopters in a compound configuration. The research described focuses on the manoeuvrability of a helicopter with an additional pusher propeller controlled by an automatic flight control system. Based on the ARCHER modular helicopter platform designed at the Warsaw University of Technology, a numerical model of the helicopter is prepared in Flightlab for one of the possible configurations with an additional pusher propeller. Subsequently, an automatic flight control system using the LQR controller to control the control of the classical part of the helicopter, and a proportional fuzzy controller to control the pitch angle and angular velocity of the additional pusher propeller is provided in the Matlab/Simulink programme. To study the manoeuvability of the object, the slalom manoeuvre described in ADS-33 is chosen, which is properly adapted to the size of the real model, based on the Froude scaling method. The study compares the results for the model equipped with an additional pusher propeller with the conventional helicopter model for different manoeuvring speeds.

Keywords: Automatic control system, compound helicopter, FLIGHTLAB, LQR, fuzzy logic

1. Introduction

Classical helicopters, understood as configurations with a single main rotor and tail rotor, are considered one of the better vessels for hovering and low-speed flight. However, they are limited by the occurrence of stall and compressibility effects on the main rotor at high flight speeds, which results in a limited range of possible achievable speeds [1]. The given restrictions could be dealt with by offloading the main rotor through reducing the required lift and thrust forces it generates. Therefore, in the 1950s, research on compound helicopter was launched to provide vessels able to flight at high speeds with simultaneous vertical takeoff and landing (VTOL) capabilities. Simultaneously, studies were conducted on the development of tiltrotors, which were also created to overcome the limitations of conventional helicopters [1].

Classical helicopters are optimal for low flight speeds and feature low rotor loads, resulting in aircraft agility that is desirable especially in military applications. On the other hand, tiltrotors also meet VTOL conditions and are designed to perform missions like fixed-wing aircraft with large forward speeds. The need for a vehicle that would complete the gap between slow and low-complexity classical helicopters and highly complex, high-speed tiltrotors was noted. Thus, the resurgence of interest in compound helicopters has been driven partly by the need for a ship that is efficient at low speeds and simultaneously able to perform missions at medium speeds in comparison with performance of classical helicopters and tiltrotors.

Since the beginning of the compound helicopters development, many configurations of these aircraft have been proposed, differing in the added subsystems to the baseline ship, the methods of

generating thrust and lift forces, as well as the methods of the drag torque compensating. The various concepts arose from the specific features of the missions for which the aircraft were dedicated. The most common configurations are compound helicopters with additional wings (lift-compounding), with push/pull propellers (thrust-compounding) and including both lifting surface and propellers (fully-compounding). The purpose of considering additional components is to reduce the lift and thrust forces generated by the main rotor. By offloading, the rotor speed could be decreased which reduces the required profile power, and the effects of stall and compressibility are shifted to occur at higher speeds, thus extending the range of speeds achievable by the aircraft.

In the lift-compounding, the aircraft is equipped with an additional wing, the purpose of which is to generate lift force during forward flight and thus increase of load factor of the aircraft. That improves efficiency at high speeds, as the wings are more effective than the rotor at highest speeds, and also improve maximal value of aircraft lift-to-drag ratio. However, a given configuration is not appropriate for lower speeds and hover, as increases hover download. The solution could be wings that rotate depending on flight conditions, however, this would add considerable complexity to the overall system. The location of the wing relative to the rotor is also important due to flow interference and is a compromise between the desired position from an operational and aerodynamic standpoint [2].

In the thrust-compounding configurations, an additional push/pull propeller is designed to generate thrust to counteract the vehicle's drag force and also act as a propulsive force, thereby relieving the main rotor in terms of propulsion force generation. That, in effect, allows forward flight at smaller fuselage angles of attack, which in theory reduces the drag of the entire helicopter. The disadvantage of the concept is the dependence of the required thrust on drag, which increases as the speed of flight increases, thus also raising the energy requirements for a given propulsion system [3]. The thrust compound configuration improves lift-to-drag ratio at higher speeds. Similar to the lift compound helicopters, the addition of a propeller complicates the system and increases the aircraft's total weight [4]. However, a given compound configuration is considered more efficient than a lift compound configuration.

Fully compound helicopters feature both propellers and wings. They could merge the advantages of both configurations. In forward flight the main rotor is aided in producing lift by the wings and in providing thrust by the propeller. This allows the main rotor to be slowed down.

In recent years, the interest in unmanned aerial vehicles (UAVs) such as helicopters and multi-rotorcraft, has increased due to their wide applicability and vertical takeoff and landing (VTOL) capabilities. UAVs were initially used exclusively for military purposes; however, with advances in technology, unmanned vehicles have become popular in civilian environments as well. Currently, they are used in such areas as military (for surveillance, reconnaissance and communication networks), disaster monitoring, environmental and resource management, aerial photography, search and rescue operations, agriculture, shipping and delivery, engineering applications, 3-D mapping, atmospheric analysis. They may be used for tasks in environments hazardous to humans [16]. UAVs are also readily used in the academic community as experimental platforms for various scientific research, including use as testbeds for learning and control algorithm. More UAV applications are listed in [5]. Helicopters are inherently unstable objects. They are characterized by nonlinear, complex, asymmetric, and coupled dynamics, which makes them perceived as more difficult to control than fixed-wing aircraft [6]. Small, unmanned helicopters are even more difficult to control than large, manned helicopters, due to the wider dynamic bandwidth of UAVs and small helicopters, their greater sensitivity to disturbances and perturbations (including from wind gusts) and to control signals [14]. Even though helicopters are very agile, they are among the most difficult to control which is due to the difficult mathematical modeling of nonlinear dynamics, and also the coupling between control inputs and vehicle state variables [7],[8]. Particularly in the case of compound helicopters, the cross-coupling that occurs between additional control surfaces can significantly affect the performance and stability of these helicopters [9]. Therefore, it is extremely essential to design reliable and robust control system that will ensure the stability of the vessel at any point of work (from the accepted possible operational range) and allow for appropriate changes in state variables to ensure that the aircraft follows a preset trajectory to accomplish a prescribed mission.

Especially nowadays, it is required to meet strict demands placed in UAVs and therefore it is neces-

sary to develop control systems that not only significantly relieve the ground pilot from remote control of the vessels, but also autonomously perform previously commanded UAVs tasks. A review of the literature providing possible solution to the unmanned, aerial vehicles control issue is presented below.

In [10] and [11] for quadcopters control the PID controllers are used, which represent a linear, conventional approach to the flight control.

In [12] an algorithm based on PID controllers and logic function for autonomous flight control in street canyons is presented.

Although the PID controllers are often used in UAVs, tuning them by trial and error is a challenging task. For this reason, in [13] is presented a method for determining optimal gains using the H₂ optimal control framework.

It has been perceived that for rotorcraft as highly complex MIMO systems, it is necessary to develop a control system that would guarantee meeting performance criteria with simultaneous consideration of physical constraints. Therefore, optimal, linear systems are considered to be preferred for MIMO systems.

The LQR, linear, optimal controller give better results than the PID, but still have poor performance on parametric uncertainties. This is because in LQR and LQG controllers, uncertainties are modeled as Gaussian white noise, and not all real uncertainties should be modeled in a particular way [16].

In [14] a tracking controller based on optimal control theory is presented for the control of a small helicopter, in which the typical LQR control issue is turned into a tracking issue.

The optimization rules related to optimal control could supplement the classical pole placement method to determine control gains, as shown in [15].

Studies described in [16] and [17] show that the linear, designed for MIMO systems H_∞ controller copes well with nonlinear objects, uncertainties in the object model and environmental disturbances. In addition, H_∞ allows the system specification to be embedded in the cost function used to synthesize the controller. In [17] the Prediction Error Minimization (PEM) helicopter identification method is used to synthesize the H_∞ controller.

In [18] for an aerobatic helicopter, using a reinforcement learning algorithm the optimal Differential Dynamic Programming (DDP) controller, an extension of the linear quadratic regulator, is used.

It is suggested in [19] that although the LQG, LQR and H_∞ optimal methods are quite good for MIMO issues they are not practical for use in aerospace environments, so the classical control approach is still used there. In the quoted work to solve the issue an algebraic approach, the Coefficient Diagram Method (CDM), is applied to the MIMO system using the LQR framework.

To overcome the disadvantages of linear controllers and to obtain controllers with an extended stability domain and increased robustness, nonlinear controllers have been developed. Nonlinear techniques could include: feedback linearization, model predictive control, dynamic inversion, adaptive control, backstepping methodology and hierarchical controller.

In [20] the PID controller is supported by a feedback linearization controller so that the control system could cope with aerodynamic effects affecting the flight of the quadrotor under conditions beyond nominal hovering conditions.

In [21] the pole placement method is used to design a linear state feedback controller for the stabilization of the helicopter in hover.

In [22] to control the flight of a small-scale rotorcraft an adaptive L₁ controller is used, which adjusts to different operating points and thus achieves speed tracking.

To solve the terrain avoidance problem, in [23] a predictive control method is used.

In [24] the issues of tracking aggressive manoeuvres of an autonomous helicopter are solved using the suboptimal, nonlinear control method of the State-Dependent-Riccati-Equation (DSRE).

In [25] a hierarchical, model-based, nonlinear controller is used to control unmanned rotorcraft and micro air vehicles. The controller transformed nonlinear mathematical models of objects into two cascaded subsystems and coupled them to each other with a nonlinear element.

Interesting solutions for unmanned aircraft control systems also included: a controller using the gradient descent optimization method presented in [26], a controller based on apprenticeship learning that uses output data from a learning algorithm shown in [27] and [28], a controller using robust and

perfect tracking (RPT) for the flight control system of a miniature unmanned rotorcraft submit in [29]. To account for the physical limitations of the actuators used on the vessels, in [30] a nested-saturation-based nonlinear controller for stabilizing the rotorcraft is proposed.

Frequently encountered hybrid systems could combine the advantages of more than one control method. Therefore in [31] an intelligent control system, which is a combination of Mamdani-type fuzzy, PID and linear controllers and which allow to achieve effective control of a small helicopter in hover and at low speeds, is presented.

Also in [32] a control system developed based on fuzzy logic, where fuzzy PID controllers are used to keep the helicopter in hover and perform simple tasks, is presented.

In [33] a linguistic, Mamdani-type of fuzzy logic controller is combined with a model-based, Takagi-Sugeno controller to control the horizontal speed of a small, unmanned helicopter. The fuzzy controller, due to its heuristic nature, is able to reflect the human pilot's experience in remotely aircraft controlling.

Proper design of the control system for a compound helicopter is also a crucial issue. In [34] for coaxial, compound helicopter the use of two, cooperative control systems is proposed: a control system typical of a helicopter for hover and low flight speeds and a fixed wing aircraft control system used at high speeds. For medium speeds in the transition mode, there is a control redundancy problem, which is solved by using a linear transition method.

To cope with complex dynamics, aerodynamic couplings between control surfaces in compound helicopters in [9] the Pi-Sigma neural network adaptive controller is used.

After performing a review of the state-of-the-art it is noticeable that quite several small UAVs in classical and multi-rotor configurations have been developed, but relatively few publications have been found that indicate a significant development of small, unmanned compound helicopters. Most of the cited works on the control of UAVs concern vessels other than compound helicopters. Systems developed for hovering and for low flight speeds are most analyzed. Few works deal with control at high flight speeds, and proposals for automatic control systems for unmanned compound helicopters are found with great difficulty.

In this paper, the development of an automatic control system for an unmanned compound helicopter is undertaken. An existing ARCHER helicopter in classical configuration, which is described in detail in [35], is used. In order to elaborate the control system, a numerical model of a classical helicopter with an additional pusher propeller fitted at the end of the tail boom is made in FLIGHTLAB programme. Thus, a thrust compound configuration is obtained. In order to test the manoeuvrability of the compound helicopter compared to the classical configuration, slalom manoeuvres are performed, during which both aircraft are controlled using an automatic flight control system developed in MATLAB/SIMULINK programme. The LQR optimal controller is selected to control the classical part of the helicopter, and in addition the pusher propeller control is connected in parallel using a fuzzy proportional controller.

The following part of the paper includes a description of the helicopter and its numerical model. Then, the control methodology and automatic flight control system are presented. Relevant test cases are shown and the results are discussed.

2. Helicopter Simulation Model

To develop the control system, the ARCHER helicopter is used. This small-scale helicopter has been created for a project conducted at the Warsaw University of Technology in 2018 and is intended to be a reconfigurable research platform to which elements such as propellers, wings and stabilators could be attached to achieve different compound helicopter configuration. The main carrier module consisting of the fuselage, propulsion unit and main rotor is built based on COTS elements [35].

In its basic configuration, the helicopter has a single main rotor and a tail propeller. The rotors are powered by separate electric motors, facilitating changes in individual rotor rotational speeds. Both rotors used in the classical ARCHER configuration are of the rigid type, as a result blade flapping is not possible.

For the purpose of this study, a pusher propeller is added to the baseline configuration, located at the end of the tail boom, while creating a thrust compound configuration. The pusher propeller could be

controlled by both rotational rate and blades collective pitch angle. As for the other rotors, the pusher propeller is also supplied by an independent electric motor.

The basic parameters of the classical ARCHER configuration are shown in table 1.

Table 1 – Basic ARCHER characteristics

Characteristic	Metric
Main rotor diameter	1,78 m
No. of MR blades	2
MR RPM	1'500 – 2'000
Tail rotor diameter	0,158 m
No. of TR blades	2
TR RPM	7'200
MR & TR rotorhubs	rigid, no flapping
TOW	8 kg
MR blades airfoil	NACA0015mod
TR blades airfoil	NACA23012
Propulsion	Electric

3. Description of the helicopter simulation model

Simultaneously with the development of the small-scale helicopter, its nonlinear, numerical model is created in the FLIGHTLAB programme, which is well-known in the industrial and academic environment to support modeling of rotorcraft, allowing to consider such aspects as dynamics, structure, aerodynamics, propulsion and control system [36]. In order to obtain a simulation model that would reflect the characteristics of a real aircraft, it is necessary to properly select the modeling methods for the various components and the load models used, which also requires considerable knowledge of rotorcraft aerodynamics.

The helicopter's main rotor is modeled as articulated. The blade element method is used to model the loads as a nonlinear function of dynamic pressure, angle of attack and Mach number. To calculate aerodynamic loads, a model of quasi-steady aerodynamic flow without stall delay is used, which utilized aerodynamic data tables containing coefficients of lift force, drag and pitching moment as a function of angle of attack and Mach number. The values of aerodynamic coefficients are validated using flight test data of the classic helicopter configuration. The Peters-He Six state model is used to determine the induced velocity. The two-blade main rotor hub is modeled as rigid, in which flapping dynamics and lead-lag blade movements are not considered. The rotor blades have a rectangular planform and are not geometrically twisted. In the model, such blade properties as position of the pitch axis, mass distribution, mass inertia moments distribution, location of the blade elements' mass centers in relation to the pitch axis are also included. The main rotor rotates in a clockwise direction. The tail and pusher propellers are modeled in a similar manner. In both cases, disc theory is used to calculate the loads, with the aim to ensuring computational efficiency for the flight control system. Both two-blade propellers are modeled as rigid. Their blades are untwisted and of zero taper ratio. The next significant modeled element is the helicopter's fuselage, which is assumed to be rigid, nonlinear and of 6 DOF. The fuselage mass properties such as total mass, center of gravity position and full inertia matrix are included in the model. To determine airloads, look-up tables are used which included aerodynamic forces and moments coefficients, which are calculated using a CFD model and are as a function of angle of attack and sideslip angle.

No interference between the propellers, rotor and fuselage is considered in the simulation model.

The airframe model also includes sensor position information and the landing gear system model. Nonlinear strut and tire models are used to model the skids. Friction of the skids against the ground is considered.

An ideal model of the propulsion system is assumed, thus for any flight conditions it is possible to deliver the required power for the helicopter.

The numerical model also includes the control system. For the basic version of the helicopter, the following four classic control variables are used: main rotor collective pitch angle, main rotor longitudinal and lateral cyclic pitch angles and tail rotor collective pitch angle. In addition, independent control of the main rotor and tail propeller speeds is provided. For the compound configuration, additional control of the pusher propeller parameters (angular rate and blade collective pitch angle) is ensured. The model omits the inertia of the control system.

It is notable that the developed helicopter numerical model also considers the parameters of the simulated flight environment. Atmospheric parameters are derived using the 1959 ARDS atmospheric model, based on hydrostatic equations and ideal gas laws. The turbulence is assumed not to occur. The nonlinear helicopter model developed in FLIGHTLAB programme contains 26 state variables:

- Helicopter fuselage: inertial position (3), velocities in body frame of reference (3), integrals of velocities in body frame of reference (3), roll, pitch and yaw angles (3), body roll, pitch and yaw rates (3), integrals of body roll, pitch and yaw rates (3),
- Main rotor: induced velocity (6) – uniform, 0th harmonic, 1st harmonics (sine and cosine), 2nd harmonics (sine and cosine),
- Tail rotor: induced flow state (1), coning angle (1).

4. Compound helicopter control

Control of a compound helicopter featuring nonlinear dynamics and couplings between channels, especially when performing more complex manoeuvres, could pose a considerable, onerous challenge for a pilot. Therefore, an automatic control system is developed to automatically guide the aircraft along a preset trajectory.

4.1 Automatic flight control

The general control system of the helicopter numerical model realized in the FLIGHTLAB programme is developed in MATLAB/SIMULINK programme. Whereas performing the flight simulation, the exchange of information between the two mentioned programmes is always ensured. The parameters of the pretrimmed helicopter in FLIGHTLAB programme are used as initial parameters in the control system, which then, utilizing the developed control laws, calculates the corresponding control variable values and sends them as input data to the helicopter's numerical model. Thus, the control signals are both output signals from the control system and input signals to the helicopter model, whereas in the reverse of that, the current values of the state vector are transmitted as output signals from the helicopter model and input signals to the control system.

In this study, an automatic control system is developed based on two controllers: an optimal, linear quadratic regulator (LQR) providing control of all measurable state variables of the helicopter and using control variables characteristic of the classical helicopter configuration, and a fuzzy proportional controller (P) providing additional parallel control of the longitudinal helicopter speed in the body frame of reference by changing the parameters of the pusher propeller - the blade pitch angle and the angular velocity.

The entire control vector, u^* , consists of the following variables:

- x_a – percentage position of the main rotor lateral cyclic stick,
- x_b – percentage position of the main rotor longitudinal cyclic stick,
- x_c – percentage position of the main rotor collective stick,
- x_d – percentage position of the tail rotor collective stick,
- x_Θ – increment of the pusher propeller blade angle in degrees,
- x_{RPM} – increment of the pusher propeller angular velocity in RPM,

The forwarded state vector, X , includes the subsequent measurable state variables:

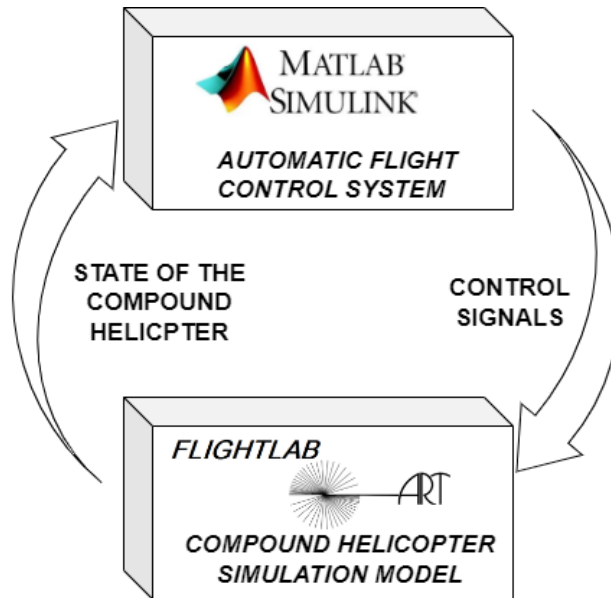


Figure 1 – Scheme of signal flow between MATLAB/SIMULINK and FLIGHTLAB.

- x, y, z - the position of the helicopter in the inertial frame of reference,
- ϕ, θ, ψ - the attitude of the helicopter in the inertial frame of reference,
- V_x, V_y, V_z - linear velocities of the helicopter in the body frame of reference,
- p, q, r - angular velocities of the helicopter in the body frame of reference.

It is worth highlighting that the presented state vector is not the full state vector used in the nonlinear helicopter numerical model, but it only consists of selected controllable state variables related to the fuselage dynamics.

Moreover, the control system includes the Stability Augmentation System (SAS), which is added to provide additional stabilization of the helicopter in the roll, pitch and yaw axis by virtue of the use of the lightweight helicopter model, which, by its small inertia, is susceptible to disturbances and control signals. The purpose of SAS is suppressing the emerging short-term angular velocity oscillations, which is accomplished by the use of three proportional controllers. The actual angular velocities (p, q, r), related to the reference, zero angular velocities and serving as input signals to the SAS, result in the determination of the control variable increments corresponding to the three control channels at the output from the stabilization system ($\Delta x_a, \Delta x_b, \Delta x_p$).

4.2 Description of the LQR controller

Application of the LQR controller requires knowledge of a linear model of the controlled object written in the form of state equations [37]:

$$\dot{X} = AX + Bu \quad (1)$$

where A and B are the state and control matrices, respectively.

Access to information about the complete state vector at any time of operation, including the initial condition, is also essential. The optimal controller operates in a feedback loop using as input the difference between the current (X) and desired (X_{des}) state vector, and taking advantage of the determined optimal feedback gain, K , which ensures the minimization of the optimal control cost function, J :

$$J = \int_0^{\infty} (X^T Q X + u^T R u) dt \quad (2)$$

where Q and R are diagonal, positively defined weight matrices of state and control, respectively and u is the control vector.

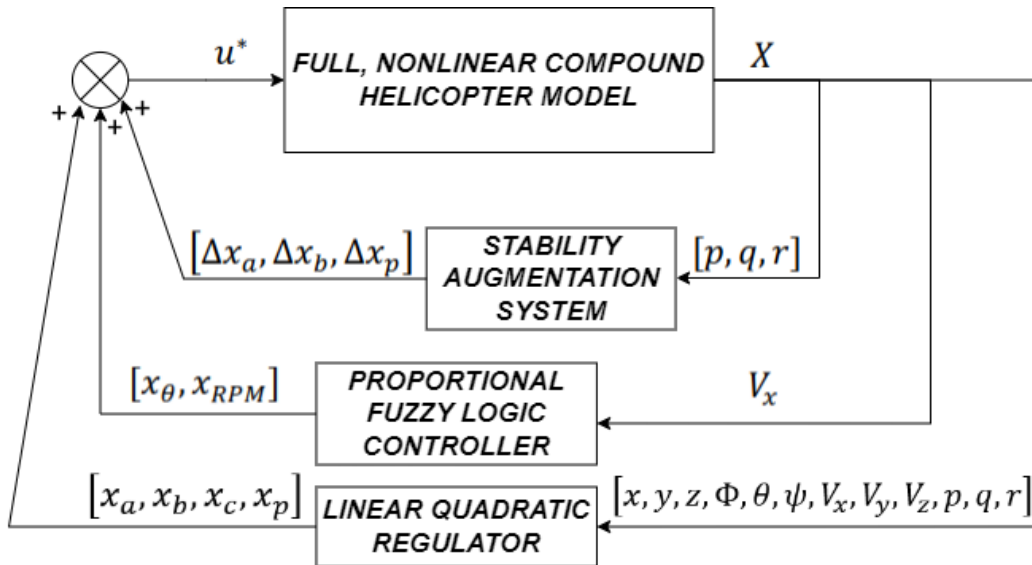


Figure 2 – Control system diagram in MATLAB/SIMULING environment.

The optimal control law is provided by the formula:

$$u = -K(X - X_{des}) \quad (3)$$

The optimal feedback gain, K , is defined by the equation:

$$K = R^{-1}B^T P \quad (4)$$

where the matrix P is determined by solving the algebraic Riccati's equation:

$$A^T P + PA - PBR^{-1}B^T P + Q = 0 \quad (5)$$

An important issue in the development of the LQR controller is the selection of the values of the weighting matrices Q and R , as they determine the character of the system's response, as well as ensure the correct and desired operation of the controller in accordance with the preset constraints and limitations. By adjusting the values of the weights, the influence of individual state and control variables on the used quality criterion can be varied and it is also possible for the controller designer to determine the degree of importance of individual states.

Thus, assuming knowledge of the linear model of the system and the values of the weight matrices, the operation of the LQR controller could be summarized as determining the control variables based on the deviation of the current state vector from the desired one and the optimal gain, which ensures minimization of the cost function.

For the purpose of this work, a linear model of the helicopter in the classical configuration is obtained by globally linearizing the full nonlinear helicopter model in the hovering condition using FLIGHTLAB programme. The resulting state matrix, A , is of dimensions 12×12 and describes the relationships between the following state variables: $x, y, z, \phi, \theta, \psi, V_x, V_y, V_z, p, q, r$, whereas the control matrix, B , of 12×4 takes into account the control variables characteristic of the classical helicopter configuration: x_a, x_b, x_c, x_p . The derived aircraft linear model is used to select the parameters of Q and R . The tuning is executed using an iterative method, during which the values of the weighting matrices are adjusted until the helicopter's expected responses to the given control signals are obtained. This requires expert knowledge of the physics of the studied phenomenon. The individual components of the Q and R matrices correspond to successive elements respectively of the state vector and control vector (when considering only the variables typical for the classical configuration). Possessing a controller developed on the basis of reduced vehicle dynamics, the LQR is applied to control the full, nonlinear helicopter model.

4.3 Description of the fuzzy controller

The fuzzy logic controller bases on uncertain sets theory, whose particular elements have some degrees of membership to the particular sets. Fuzzy controller is static, nonlinear controller. By assigning characteristic functions of membership value for input and output signals, and creating proper control roles, which define the relationships between input signals and desired outputs, controller designer may create a customized response basing on the own experience, without knowing the exact dynamics of the object. This allows to proceed from quantitative to qualitative description of the model. The process on which the controller determines the system's response consists of three individual steps [38]:

- Fuzzification consists in determining the degrees of membership of individual fuzzy sets for the input signals of the controller. Before it is done, scaling is performed. It involves multiplying the physical input value by a normalization factor, in such a form, it is transformed into a normalized input domain.
- Interference relies on determining degrees of membership, the inference block determines fuzzy regulatory decisions. This is done on the basis of the adopted control rules.
- Defuzzification is the reverse process of fuzzification and involves determining the acute numerical values for each control variable, according to the fuzzy control decisions developed in the inference block. Each control variable shall have only one assigned value. Following the defuzzification, a denormalization is performed, which is the multiplication of the normalized output value by the denormalization factor. It puts the variable into the physical output domain [38].

Fuzziness is defined by its membership functions which are a nonnegative-valued functions. In contrast to the probability density functions, the area under the curve of a membership function may not be equal to unity. One of the main features of fuzzy set theory is, that a member of a fuzzy set may assign more than one membership values, that may be even conflicting. Such a description of a fuzzy set is very useful in many real-world applications. More importantly, the use of conflicting membership functions does not create any logical or mathematical problems in the fuzzy controller. However, a correct approach to the given problem must be taken [39].



Figure 3 – Process of determining response of fuzzy logic controller.

The membership functions might be created by graphical representations. It can consist of various different shapes. The most common ones are: triangular, trapezoidal, rectangular, piecewise linear, Gaussian, type-Z, type-S [40].

For the proposed control system, an additional fuzzy proportional (P) controller is implemented to simultaneously control both the RPM and pitch of the pusher propeller in parallel with the LQR controller. The input signal is the difference in the preset and the current forward speed, while at the output the controller produces a correction in the form of an increase or decrease in RPM and pitch, which is fed back to the model in a feedback loop. Three different overlapping membership functions are designed for the input: Type-Z and Type-S to represent the speed deviation (longitudinal speed either too low or too high) and a Gaussian function to cover the desired state of the preset speed. Both outputs use type-Z and type-S membership functions, together with a triangular membership functions for the medium range of angular speeds and pitch angles of the pusher propeller.

5. Test cases

After developing the numerical model of the compound helicopter, an important issue is to prove its manoeuvrability, namely the capacity to change the aircraft's flight path by exerting forces from the

rotor and propellers [41]. In order to accomplish this, the slalom manoeuvres defined in the Aeronautical Design Standard 33 (ADS-33) as one Mission Task Element (MTE) is used [42]. The selected MTE, due to the requirement for rapid and sustained manoeuvring, allows to assess the aircraft agility, and also to determine the helicopter responsiveness, including the control effectiveness with the use of the proposed automatic control system.

The aforementioned specification, which is elaborated for manned helicopters, in recent years has been recognized as the most comprehensive group of requirements for manoeuvrability, agility and handling qualities. However, in most cases, the metrics included in ADS-33 cannot be directly applied to small, unmanned aircraft [41]. Thus, in the presented study, due to the performance of flight by an unmanned, small aircraft, the parameters of the set manoeuvre require modification. This is accomplished by proportionally reducing the preset distances between successive points in space (from 500 ft and 50 ft to 100 ft and 10 ft, respectively) while maintaining the nature of the slalom trajectory. Considering the Froude scaling method [43], which is used to adapt the criteria contained in ADS-33 to small-scale rotorcraft, and in which the length scaling factor (N) is the quotient of the characteristic dimensions of the full-scale, reference helicopter and the examined helicopter (in this work it is the ratio of the main rotors' diameters: $N = D_{ref}/D_{ARCHER}$), the assumed value of the length scaling factor $N = 5$ might be justified as properly established, since, with the ARCHER's main rotor diameter $D_{ARCHER} = 1.78$ m, the characteristic dimension of the reference helicopter should be $D_{ref} = 8.9$ m, which is a value within the typically encountered range of main rotor diameters of manned civil helicopters. Considering the requirements of ADS-33 for Degraded Visual Environment, the maintained airspeed should be at least 22,64 ft/s, where the velocity scaling factor used is \sqrt{N} .

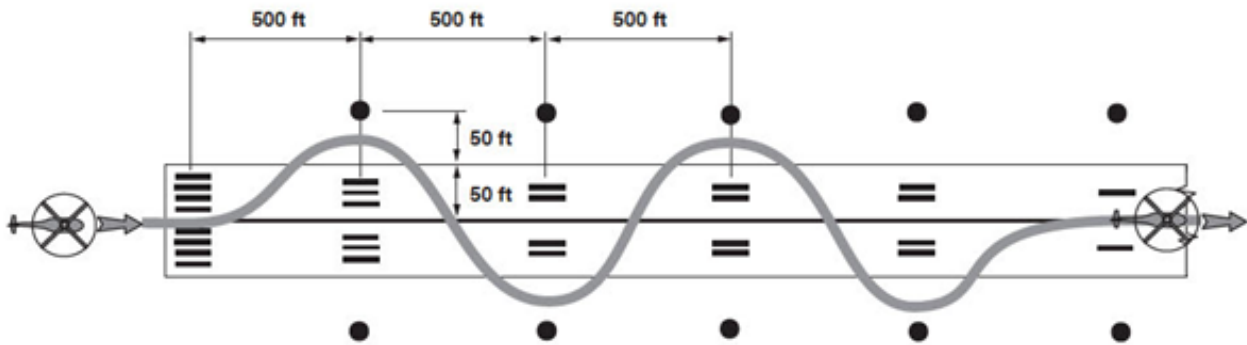


Figure 4 – Original trajectory of the slalom manoeuvre defined in ADS–33 [42].

In the developed system, the trajectory of the manoeuvre is defined in the form of preset points in space, which should be successively reached by the aircraft, and which are spaced from each other in the longitudinal direction by 100 ft and in the lateral direction by $2 \cdot 10$ ft.

Subsequently, to conduct an automatic flight along the designed path the developed control system is used. The manoeuvring capabilities of the helicopter without and with an additional pusher propeller are compared for various assumed, constant values of forward speeds, $V_{x_{des}}$. This is done using appropriately planned test cases (table 2).

Table 2 – Test cases

No. / Figure	Helicopter configuration	Set forward speed [ft/s]
1/Fig.5	Classical (without pusher propeller)	10
2/Fig.6		20
3/Fig.7		30
4/Fig.8		40
5/Fig.9	Compound (with pusher propeller)	10
6/Fig.10		20
7/Fig.11		30
8/Fig.12		40

At the initial time of the simulations, the helicopter is trimmed to hover with an absolute attitude (z position coordinate) of 100 ft and with zero horizontal position coordinates (x and y) in an inertial frame of reference. In each case, the aircraft first accelerates from the hovering state to a specified forward speed value, and then starts executing the target slalom manoeuvre. On the flight control system are imposed the requirements of maintaining a constant flight altitude and a preset forward speed in body frame of reference (once it is reached). During the simulation, the operation of the entire control system described in Chapter IV is shown. For individual test cases, the settings of the used controllers are identical and do not change.

In cases 1 – 4 the behavior of the helicopter in the classical configuration while performing the selected manoeuvre at four preset forward speeds (10, 20, 30 and 40 ft/s) is examined. Whereas in cases 5 – 8, corresponding flight simulations with the use of a compound helicopter are conducted. Shown in figures 5 – 12 the helicopter's time-function responses for following test cases include: position in the inertial frame of reference (X, Y, Z), attitude in the inertial frame of reference ($Phi, Theta, Psi$), linear velocities in the body frame of reference (V_x, V_y, V_z), angular velocities (P, Q, R) and control variables for classical and compound configurations.

In the paper, two criteria from the specification are expanded to include four requirements for the other components of position and flight speed. In addition, to quantitatively evaluate the achieved position and maintained flight speeds, the developed reference values of the mentioned quantities are compared with the actual helicopter position and speed values obtained from simulation using the Root Mean Square (RMS) criterion.

The reference quantities are defined as follows:

- $V_{x_{ref}}$ – the reference velocity component V_x is constant and equal to the set $V_{x_{des}}$ value,
- $V_{y_{ref}}$ – the reference velocity component V_y is constant and equal to zero,
- $V_{z_{ref}}$ – the reference velocity component V_z is constant and equal to zero,
- X_{ref} – the reference position component X is an integral over a simulation time of derived transformation formula of reference velocity $V_{x_{ref}}$ from body to earth frame reference:

$$X_{ref} = \int_0^t \left(V_{x_{ref}} \cdot \cos(Theta) \cdot \cos(Psi) + V_{y_{ref}} \cdot (\sin(Phi) \sin(Theta) \cos(Psi) - \cos(Phi) \sin(Psi)) + V_{z_{ref}} \cdot (\cos(Phi) \sin(Theta) \cos(Psi) + \sin(Phi) \sin(Psi)) \right) dt \quad (6)$$

Assuming that $V_{y_{ref}}$ and $V_{z_{ref}}$ are equal to zero, as described above, the final reference position formula resulting from the component V_x in converted to the following equation:

$$X_{ref} = \int_0^t \left(V_{x_{ref}} \cdot \cos(Theta) \cdot \cos(Psi) \right) dt \quad (7)$$

where $V_{x_{des}}$ is the set longitudinal velocity in the body frame of reference, $Theta$ and Psi are the actual pitch and roll angles, respectively and t is the flight time. For the time corresponding to the rise of the actual speed value from zero to the set one, the aircraft's current speed in body frame of reference is used in the given formula,

- Y_{ref} - the reference position component Y is defined as zero value for the points when the aircraft enters and exits the slalom and as a sine wave for the moment when the manoeuvre is executed, which could be determined by the formula:

$$Y_{ref} = \begin{cases} 10 \cdot \sin\left(\frac{x}{20\pi + \pi/3,78} + \frac{3\pi}{2}\right) & \text{for } 100 \text{ ft} \leq X \leq 200 \text{ ft} \\ 10 \cdot \sin\left(\frac{x}{10\pi + \pi/7,57} - \frac{3\pi}{2}\right) & \text{for } 200 \text{ ft} \leq X \leq 500 \text{ ft} \\ 10 \cdot \sin\left(\frac{x_{ref}}{20\pi + \pi/3,78} - 3\pi\right) & \text{for } 500 \text{ ft} \leq X \leq 600 \text{ ft} \\ 0 & \text{for } X \leq 100 \text{ ft or } X_{ref} \geq 600 \text{ ft} \end{cases} \quad (8)$$

- Z_{ref} - the reference position component Z is constant with an absolute value of 100 ft.

The Root Mean Square criterion is given by the following formula [44]:

$$RMS = \sqrt{\frac{1}{n} \sum_{k=1}^n (\chi_{ref,k} - \chi_k)^2} \quad (9)$$

$$RMS_{pos} = \sqrt{\frac{1}{n \cdot p} \sum_{j=1}^p \sum_{k=1}^n (\chi_{ref,j,k} - \chi_{j,k})^2} \quad (10)$$

$$RMS_{vel} = \sqrt{\frac{1}{n \cdot p} \sum_{j=1}^p \sum_{k=1}^n (\chi_{ref,j,k} - \chi_{j,k})^2} \quad (11)$$

where: RMS , RMS_{pos} , RMS_{vel} are the criterion value of the considered state variable χ , position and velocity respectively, k is the time step resulting from the simulation data logging period, n is the total number of time steps resulting from the simulation duration, $\chi_{ref,k}$ and χ_k are the reference and actual values of the state variable at the k^{th} time step, respectively, j is the number of the currently compared component out of all $p = 3$ collated variables.

It is worth highlighting that the calculation of the RMS parameter should start when the helicopter reaches the set $V_{x_{des}}$ values.

6. Results

The helicopter responses in the selected test cases are shown in the following figures 5 – 12. The black color indicates the current values of the state and control variables, whereas the red color indicates the reference values of the position coordinates and speed components. Additionally, the comparison of the actual and reference Y coordinates as a function of the X coordinate is shown in the 13 - 16 figures. The exact values of the RMS criterion are provided in table 3.

Table 3 – Values of the RMS parameters

Test Case No.	RMS_x [ft]	RMS_y [ft]	RMS_z [ft]	RMS_{V_x} [ft/s]	RMS_{V_y} [ft/s]	RMS_{V_z} [ft/s]	RMS_{pos} [ft]	RMS_{vel} [ft/s]
1	25.41	2.47	0.17	1.07	0.43	1.99	2011.56	272.02
2	16.41	4.37	0.42	3.09	2.20	2.12	1130.88	377.36
3	9.81	6.44	1.01	4.53	5.26	3.76	612.47	473.42
4	18.45	7.80	1.60	4.43	8.02	5.86	772.03	591.11
5	21.01	2.66	0.70	0.44	2.73	2.14	1689.20	408.83
6	12.51	5.23	1.19	1.11	4.80	2.00	946.63	464.79
7	21.23	8.19	1.70	2.57	7.32	3.41	1090.41	553.18
8	6.91	9.04	2.52	2.47	9.92	4.29	630.42	638.15

- Forward speed: $V_{x_{des}} = 10 [ft/s]$ – Cases 1 and 5

For the cases at a forward speed V_x of 10 ft/s, it can be seen that the model performs the manoeuvre correctly, the initial lateral deviation is 2 ft for both cases, however, during the manoeuvres, the maximum overshoot at the points where the object should be at the extreme positions from the central axis does not exceed 0.1 ft. The maximum delay in achieving the extreme points relative to the X position is 5 ft for both cases. It can be concluded that in terms of trajectory, both systems for a given speed V_x of 10 ft/s exhibit comparable flight characteristics. Similar observation can be made by observing the graph presenting the altitude during the manoeuvres, for the object using a pusher propeller, the error in altitude is constant at 0.7 ft, while without a pusher propeller, it varies in the range of +0.2 ft to -0.3 ft. The largest difference between the two cases is considered for the velocity V_x in the body frame of reference, The model with a pusher propeller shows greater stability in terms of maintaining the set velocity $V_{x_{ref}}$, the error for the case with a pusher propeller does not exceed 0.2 ft/s while, the model

without a pusher propeller is characterized by a much larger discrepancy, reaching a maximum error of more than 4 ft/s.

- Forward speed: $V_{x_{des}} = 20 [ft/s]$ – Cases 2 and 6

As the speed V_x increases from 10 ft/s to 20 ft/s, a deterioration in the coverage of the actual flight trajectory with the reference trajectory is seen for both cases. As for the speed of 10 ft/s, the initial deviation before the start of the manoeuvre is 2 ft. During the manoeuvre the maximum deviation of the Y position in respect of the reference trajectory is 3 ft, while at the turning points it reaches 2 ft. The maximum error of the Y position at the points of greatest deviation from the central axis does not exceed 0.2 ft for the case without a pusher propeller, while for the case with a pusher propeller this error does not exceed 0.1 ft. For both cases reaching the turning points is delayed in relation to the X position by a value of 30 ft. Altitude maintenance for a flight speed of 20 ft/s has similar tendency to that for a speed of 10 ft, however the differences from the reference value are greater. For the case without a pusher propeller, the altitude varies from 99 ft to 101 ft, while the altitude for the case with a pusher propeller maintains a value of 101 ft with a maximum variation of 0.5 ft. In terms of linear velocity V_x , large speed fluctuations are observed for the case without the pusher propeller, the velocity reaches a value as high as 30 ft/s in a certain range, which gives a relative error from the reference value of 50%. For the case with a pusher propeller, the maximum error in a certain range is 4 ft/s which gives an error of 20%.

- Forward speed: $V_{x_{des}} = 30 [ft/s]$ – Cases 3 and 7

For the cases 3 and 7 with a V_x speed of 30 ft/s, there is a further deterioration in the coverage of the desired flight trajectory with the actual one, increasing the delay of the actual Y position with the reference position by 40 ft for the object without a pusher propeller and 60 ft for the case with a pusher propeller in respect to the X position. No significant overshoot of the Y position values at the turning points was noticed, in comparison to the results for V_x of 20 ft/s. The error in Y position in relation to the reference trajectory reaches 10 ft for both cases, this is due to the delay of the model in relation to the reference trajectory in X position. The altitude for the model with a pusher propeller varies from a value of 97 ft to 103 ft, while for the model without a pusher propeller, the value oscillates in the range of 98 ft to 102 ft. It is worth noting that, in contrast to the cases with lower speeds V_x , the differences in speed variations from the reference value are comparable for both cases 3 and 7 and reach a value of up to 40 ft/s, which gives an error of 33%, apart of that, with the use of a pusher propeller, the model reaches the set speed faster: 2 seconds, compared to 5 seconds for the case without the pusher propeller.

- Forward speed: $V_{x_{des}} = 40 [ft/s]$ – Cases 4 and 8

At a speed V_x of 40 ft/s, the model is unable to track the set manoeuvre for both described cases. For the model without a pusher propeller, the object is unable to follow the manoeuvre at the second turn, reaching a maximum value of 7 ft from the central axis, at a delay relative to the X position of 80 ft, while for the model with a pusher propeller the delay reaches a value of 100 ft and stops following the set trajectory at the third turn reaching a maximum value of the Y position of 6 ft. The altitude for the model without a pusher propeller varies for the manoeuvre between 95 ft and 103 ft, while for the model with a pusher propeller the range is between 99 ft and 106 ft. In the case of maintaining the reference speed V_x , there is an analogous situation to the case at 30 ft/s. No significant differences were observed between the 4 and 8 cases, the value of the maximum deviation is 10 ft/s, and reaches a value of 50 ft/s. However, it is possible to observe a deepening trend from the cases for the speed V_x of 30 ft/s. The model with a pusher propeller reaches the set speed in 3 seconds, while the model without a pusher propeller requires 7 seconds. Moreover, case 4 shows a tendency to lag the set speed, in contrast to case 8. Analyzing the results obtained for V_x 40 ft/s, it seems pointless to perform tests for higher speeds V_x .

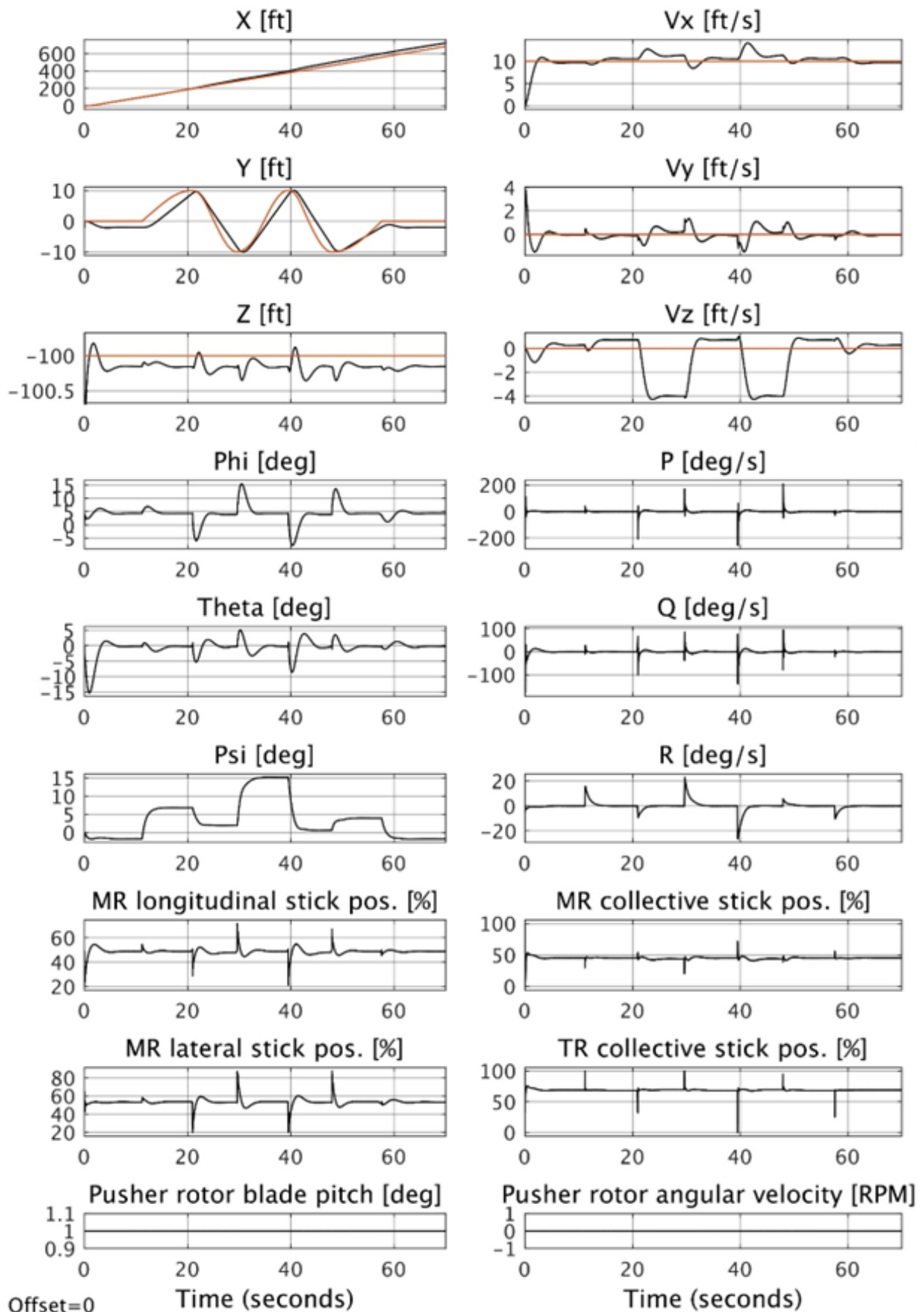


Figure 5 – Helicopter response for case 1.

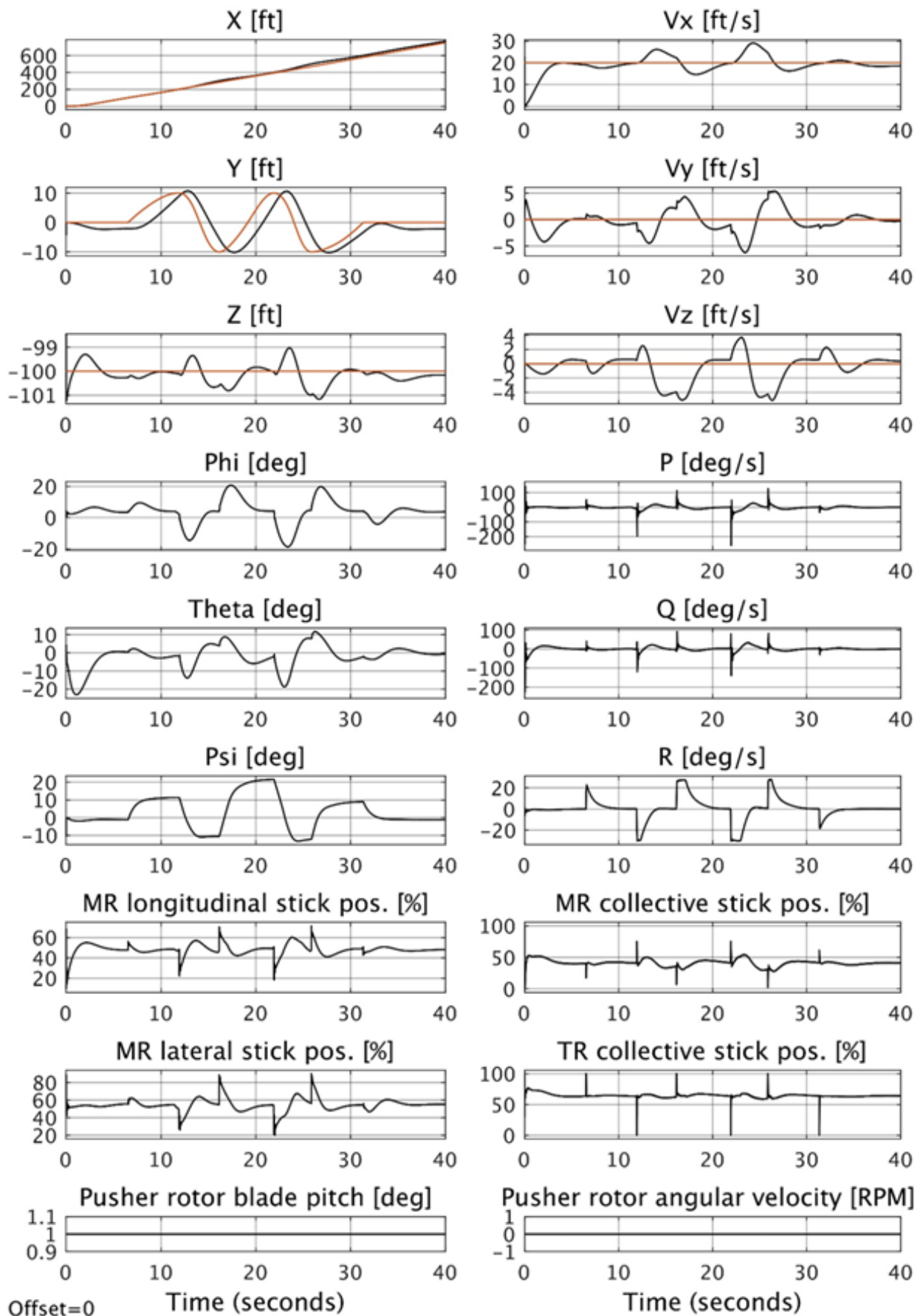


Figure 6 – Helicopter response for case 2.

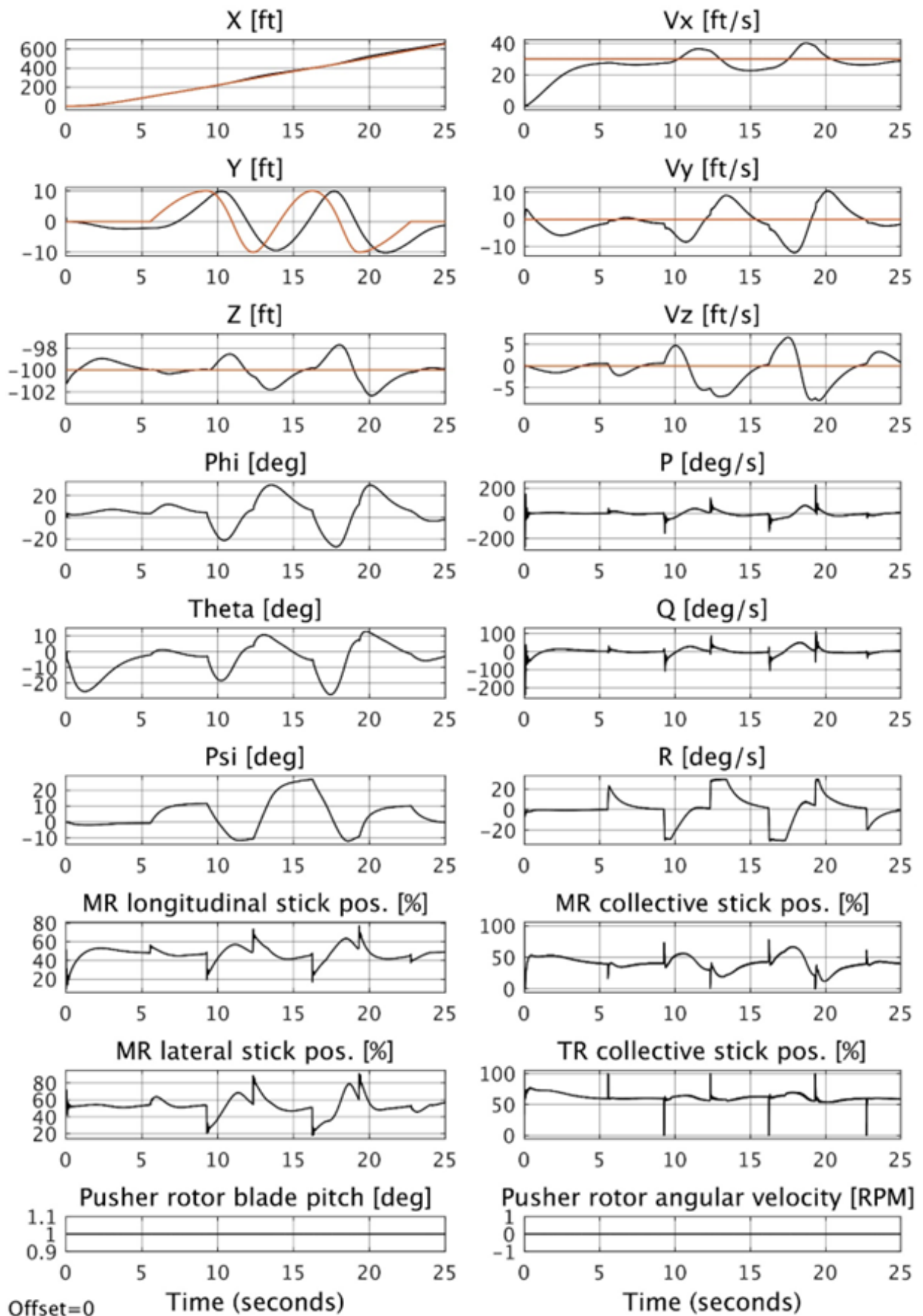


Figure 7 – Helicopter response for case 3.

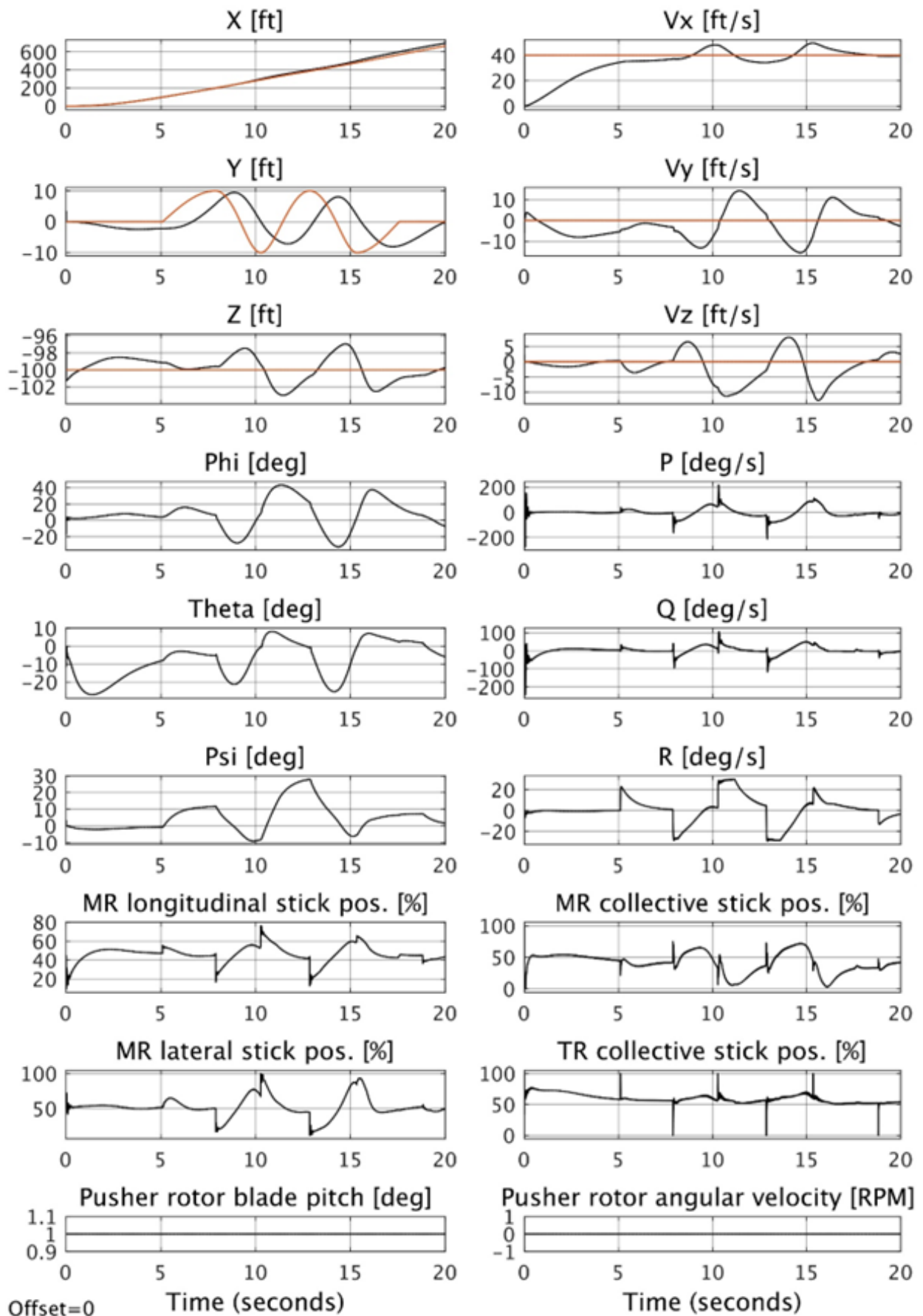


Figure 8 – Helicopter response for case 4.

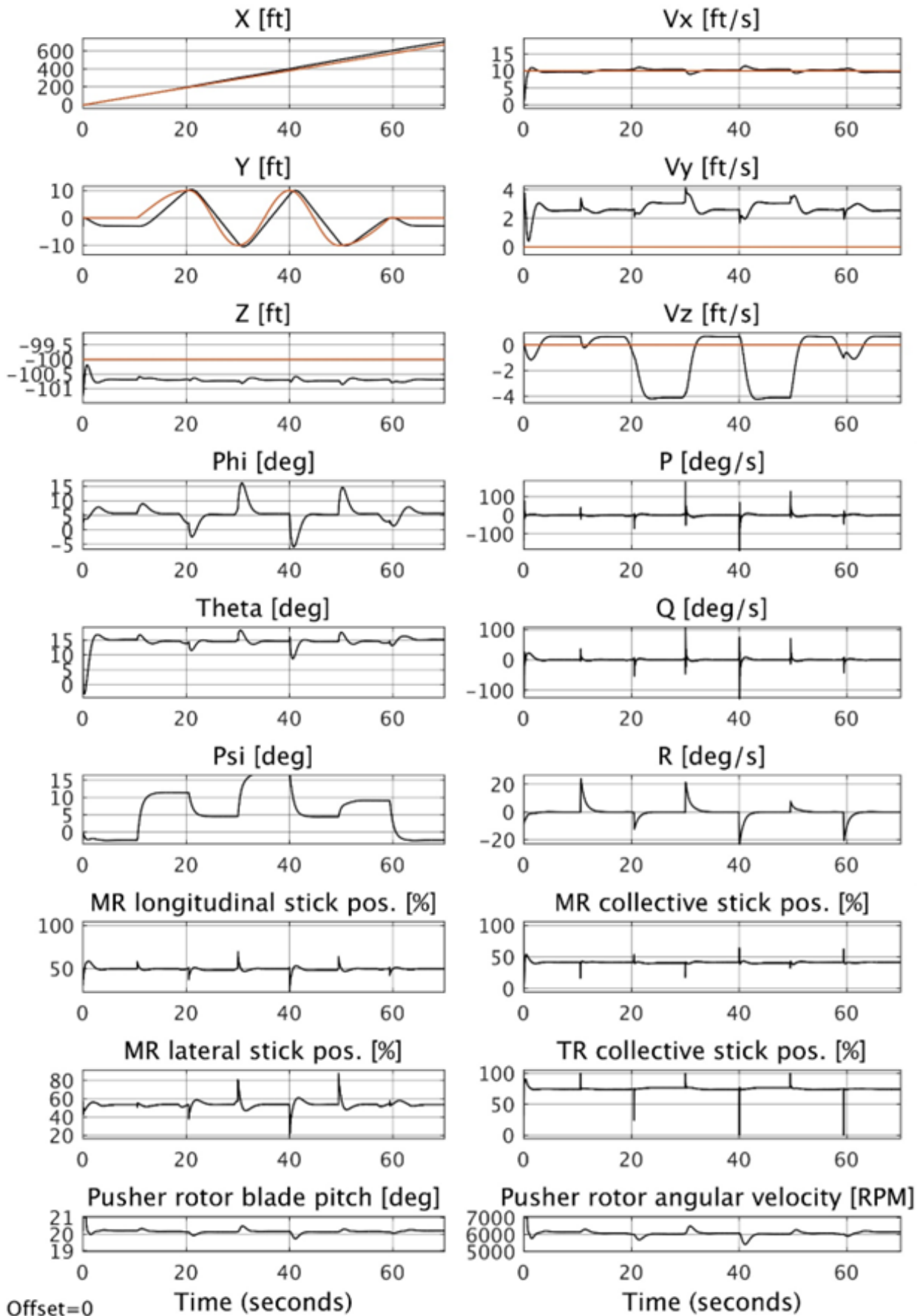


Figure 9 – Helicopter response for case 5.

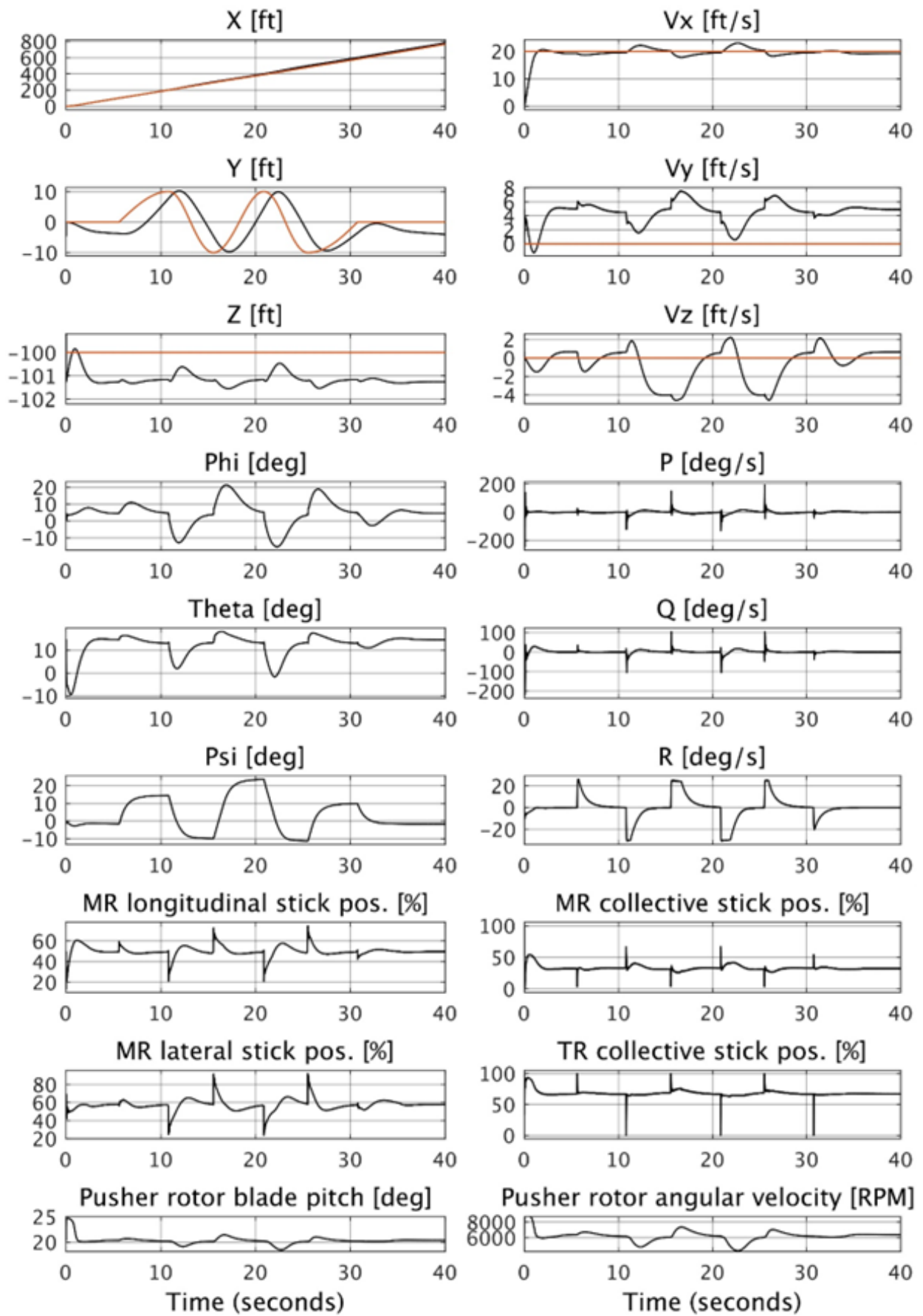


Figure 10 – Helicopter response for case 6.

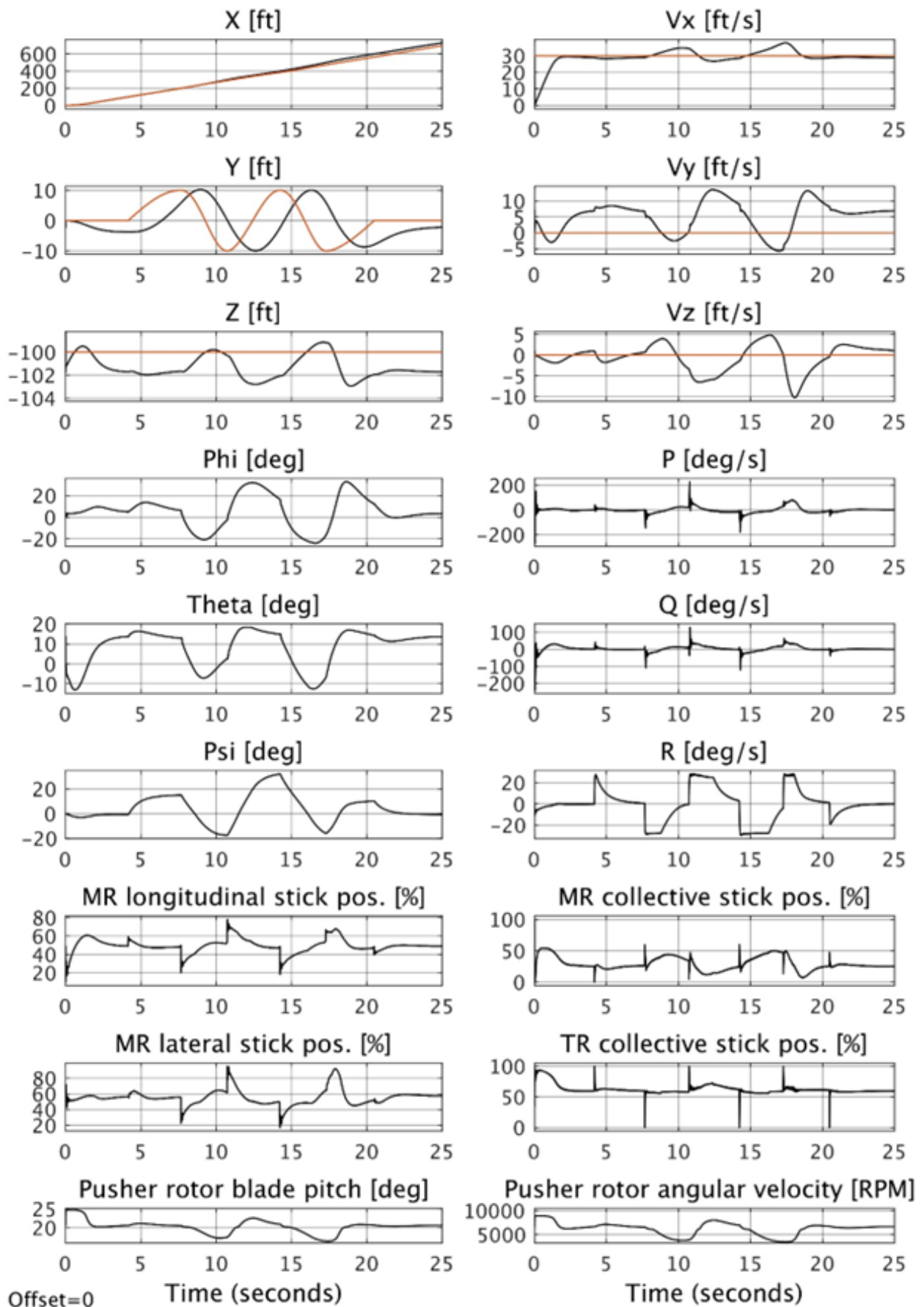


Figure 11 – Helicopter response for case 7.

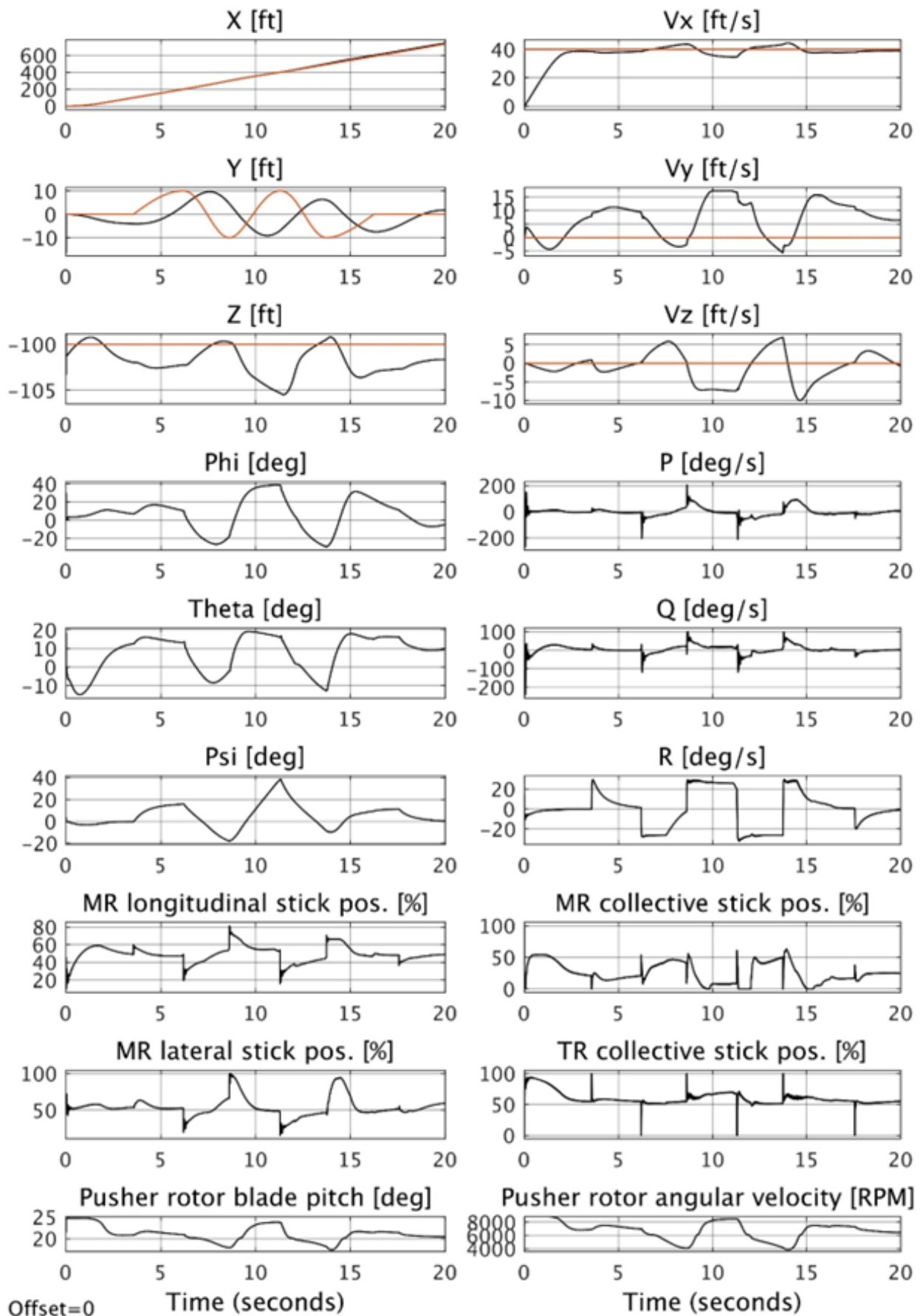


Figure 12 – Helicopter response for case 8.

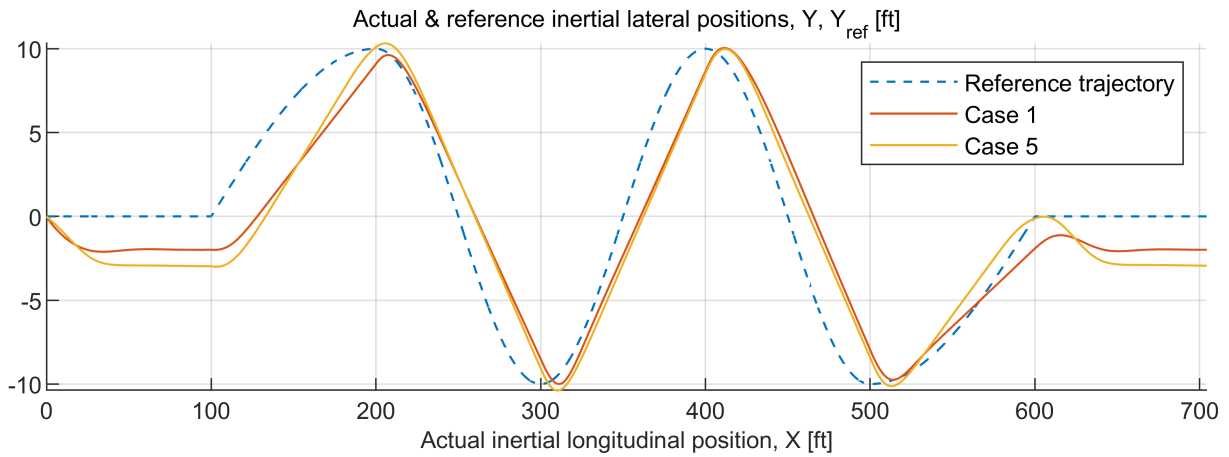


Figure 13 – Two–dimensional plot of the current and reference slalom trajectory for the case 1 and 5.

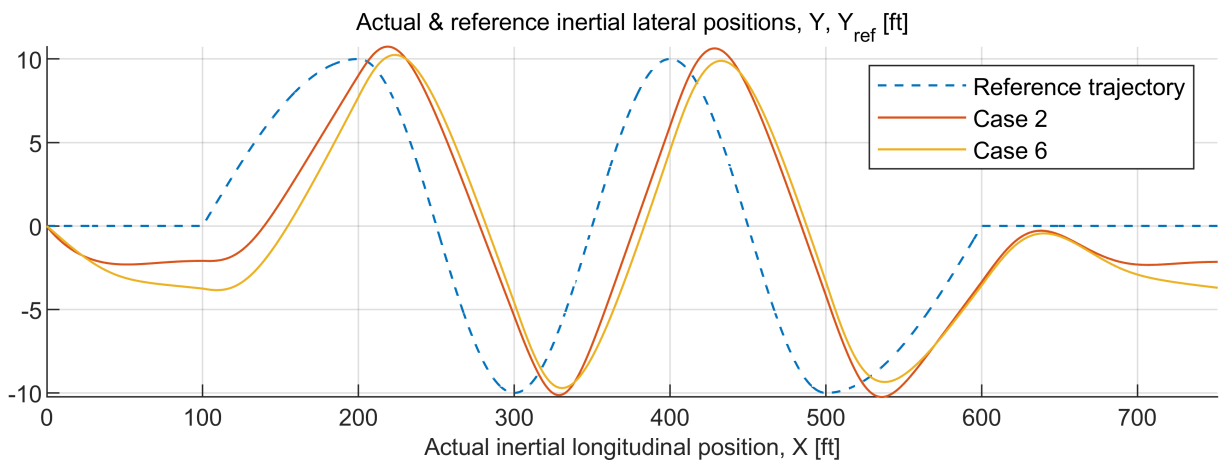


Figure 14 – Two–dimensional plot of the current and reference slalom trajectory for the case 2 and 6.

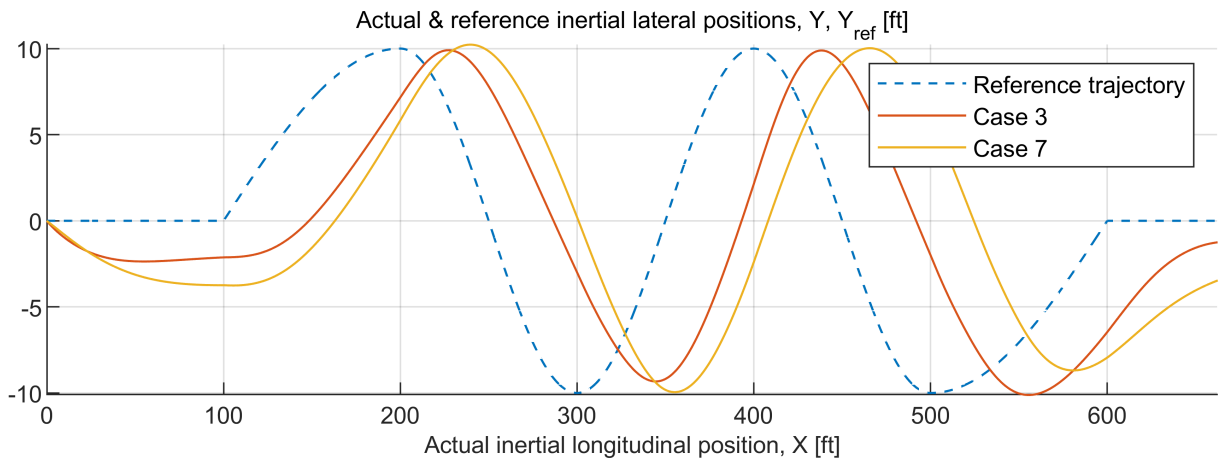


Figure 15 – Two–dimensional plot of the current and reference slalom trajectory for the case 3 and 7.

Analyzing the results obtained from the RMS parameters for all the cases, it can be seen that the model without a pusher propeller has a better coverage of the reference trajectory in the Y position than for the object with a pusher propeller, over the whole range of speeds V_x tested in this study. In terms of trajectory coverage in the X position, the model with a pusher propeller shows better characteristics. This is due to a lower tendency to fly in the slipstream compared to the second object. When analysing the altitude maintenance, the model without pusher propeller shows lower values of the RMS parameters. However, when comparing the actual error values from the individual case plots, it can be concluded that both models maintain very similar characteristics. It is found that

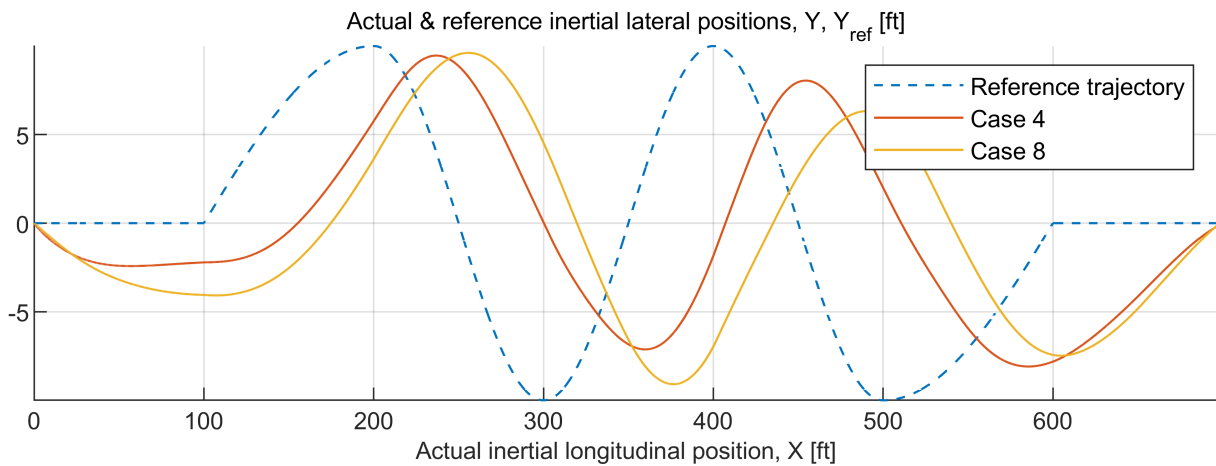


Figure 16 – Two–dimensional plot of the current and reference slalom trajectory for the case 4 and 8.

in the case of using a pusher propeller the object is more stable in respect of maintaining the set speed V_x . In the RMS calculations the initial acceleration was not taken into account, therefore the results presented in the table above refer only to the speed deviation during the manoeuvre. Finally, it should be noted that when analysing the RMS for the overall position, the model with the pusher propeller performs more effectively for the speed range of 10-20 ft/s, after which the RMS value for the speed of 30 ft/s is lower for the helicopter without the pusher propeller. No clear conclusions can be drawn from the RMS_{pos} results for the speed V_x of 40 ft/s, as both models were unable to perform the set manoeuvre at this speed.

7. Conclusion

The paper presents development of the automatic flight control system dedicated for the compound helicopter equipped with additional pusher propeller. The nonlinear helicopter model developed in FLIGHTLAB programme is used for implementing the integrated control algorithm based on LQR to control the conventional part of the helicopter and a proportional fuzzy controller to regulate the angular velocity and pitch of the additional pusher propeller.

The efficiency of the developed control system was checked by using slalom manoeuvre described in the Aeronautical Design Standard 33 as reference flight trajectory and conditions. Due to the helicopter scale, appropriate corrections were made to the trajectory of the manoeuvre based on the Froud scaling method. Eight tests were performed for different helicopter configurations (with and without the pusher propeller) and flight conditions, allowing to quantitatively assess the helicopter control effectiveness. It was observed that the model with a pusher propeller showed a number of advantages over the classical configuration, such as better stability in terms of maintaining the preset forward speed, or better coverage of the slalom trajectory for low-speed flights. The general conclusion of the study is that the proposed control system can be used efficiently for selected compound helicopter configuration.

Possibilities of further studies are broad. However, as a next step, it is decided to analyze power consumption for both classical and compound helicopter configurations.

8. Contact Author Email Address

Sara Waśniewska: sara.wasniewska.dokt@pw.edu.pl

9. Copyright Statement

The authors confirm that they, and/or their company or organization, hold copyright on all of the original material included in this paper. The authors also confirm that they have obtained permission, from the copyright holder of any third party material included in this paper, to publish it as part of their paper. The authors confirm that they give permission, or have obtained permission from the copyright holder of this paper, for the publication and distribution of this paper as part of the READ proceedings or as individual off-prints from the proceedings.

References

- [1] Ormiston R A. Revitalising advanced rotorcraft research – and the compound helicopter. *The Aeronautical Journal*, Vol. 120, No. 1223, pp 83-129, 2016. doi:10.1017/aer.2015.5.
- [2] Yeo H. Design and aeromechanics investigation of compound helicopters. *Aerospace Science and Technology*, Vol. 88, pp 158-173, 2019. DOI: 10.1016/j.ast.2019.03.010.
- [3] Ferguson K, Thomson D. Performance comparison between a conventional helicopter and compound helicopter configurations. *The Institution of Mechanical Engineers Part G Journal of Aerospace Engineering*, Vol. 229, No. 13, 2015. DOI 10.1177/0954410015577997.
- [4] Blacha M, Fink A, Eglin P, Cabrit P. „Clean sky 2”: exploring new rotorcraft high speed configurations. *The 43rd European Rotorcraft Forum*, Milan, Italy, 2017.
- [5] Koldaev A V. Non-military UAV applications. 2007.
- [6] Leishman J G. *Principles of helicopter aerodynamics*. 1st edition, Cambridge University Press, 2000.
- [7] Krol D, Lower M, Szlachetko B. Helicopter intelligence in hover: quality improvement of the fuzzy regulator. *The Sixth International Conference on Intelligent Systems Design and Applications (ISDA 2006)*, Jinan, China, 2006. DOI: 10.1109/ISDA.2006.167.
- [8] Camilleri M, Scerri K, Zammit S. Autonomous flight control for an RC helicopter. *2012 16th IEEE Mediterranean Electro-technical Conference*, Yasmine Hammamet, Tunisia, pp 391-394, 2012. DOI: 10.1109/MELCON.2012.6196456.
- [9] Zheng F, Xiong B, Zhang J, Zhen Z, Wang F. Improved neural network adaptive control for compound helicopter with uncertain cross-coupling in multimodal maneuver. *Nonlinear Dynamics*, Vol. 2022, Vol. 108, No. 4, pp 3505-3528, 2022. DOI: 10.1007/s11071-022-07382-x.
- [10] Bayisa A T. Controlling quadcopter altitude using PID-control system. *International Journal of Engineering Research & Technology (IJERT)*, Vol. 8, No. 12, 2019. DOI: 10.17577/IJERTV8IS120118.
- [11] Usman M. Quadcopter modelling and control with MATLAB/Simulink implementation. Bachelor's Thesis, Mechanical Engineering and Production Technology, LAB Univ. of Applied Sciences, Lappeenranta, Finland, 2020.
- [12] Kownacki C. Study of flight control algorithm of micro aerial vehicle in unknow urban environment. *Acta Mechanica et Automatica*, Vol.4, No. 3, pp 87-93, 2010.
- [13] Kim S, Deshpande V M, Bhattacharya R. H2 optimized PID control of quadcopter platform with wind disturbance. *2020 International Conference on Unmanned Aircraft Systems (ICUAS)*, Athens, Greece, pp 839-844, 2020. DOI: 10.1109/ICUAS48674.2020.9214010.
- [14] Budiyo A, Wibowo S S. Optimal tracking controller design for a small scale helicopter. *Journal of Bionic Engineering*, Vol. 4, No. 4, pp 271-280, 2007. [https://doi.org/10.1016/S1672-6529\(07\)60041-9](https://doi.org/10.1016/S1672-6529(07)60041-9).
- [15] Hua M D, Hamel T, Morin P, Samson C. Introduction to feedback control of underactuated VTOL Vehicles: A review of basic control design ideas and principles. *IEEE Control System*, Vol. 33, No. 1, pp 61-75, 2013. DOI: 10.1109/MCS.2012.2225931.
- [16] Tijani I B, Akmeliawati R, Legowo A, Budiyo A, Abdul Muthalif A G. H ∞ robust controller for autonomous helicopter hovering control. *Aircraft Engineering and Aerospace Technology*, Vol. 83, No. 6, pp 363-374, 2011. DOI: 10.1108/00022661111173243.
- [17] Dharmayanda H R, Budiyo A, Kang T. State space identification and implementation of H ∞ control design for small scale helicopter autonomous quadrotor helicopters. *Journal of Aircraft Engineering and Aerospace Technology*, Vol. 82, No. 6, pp 340-352, 2010. DOI:10.1108/00022661011104493.
- [18] Abbeel P, Coates A, Quigley N, Ng A Y. An application of reinforcement learning to aerobatic helicopter flight. *Advances in Neural Information Processing Systems*, Vol. 19, 2007.
- [19] Budiyo A, Sudiyanto T. An algebraic approach for the MIMO control of small scale helicopter. *CoRR*, 2008. DOI: 10.48550/arXiv.0806.4648.
- [20] Huang H, Hoffmann G M, Waslander S L, Tomlin C J. Aerodynamics and control of autonomous quadrotor helicopters in aggressive maneuvering. *IEEE International Conference on Robotics and Automation*, 2009. DOI: 10.1109/ROBOT.2009.5152561.
- [21] Wahab A A, Mamat R, Shamsudin S S. Control system design for an autonomous helicopter model in hovering using pole placement method. *International Journal of Integrated Engineering*, 2013.
- [22] Guerreiro B J, Silvestre C, Cunha R. L1 Adaptive control for autonomous rotorcraft. *The 2009 American Control Conference Hyatt Regency Riverfront*, St. Louis, MO, USA, 2009.
- [23] Guerreiro B, Silvestre C, Cunha R. Terrain avoidance model predictive control for autonomous rotorcraft. *The 17th International Federation of Automatic Control World Congress*, Seoul, Korea, 2008.
- [24] Geranmehr B, Khanmirza E, Kazemi S. Trajectory control of aggressive maneuver by agile autonomous

- helicopter. *Proceedings of the Institution of Mechanical Engineers, Part G: Journal of Aerospace Engineering*, Vol. 233, No. 4, pp 1526-1536, 2018. DOI: 10.1177/0954410018755807.
- [25] Kendoul F, Yu Z, Nonami K. Guidance and nonlinear control system for autonomous flight of mini-robotcraft unmanned aerial vehicles. *Journal of Field Robotics*, Vol. 27, No. 3, pp 311-334, 2009. DOI: 10.1002/rob.20327.
- [26] Kadmiry B, Palm R, Driankov D. Autonomous helicopter control using gradient descent optimization method. *The 4th Asian Conference on Robotics and its Applications* Singapore, 2001.
- [27] Coates A, Abbeel P, Ng A Y. Apprenticeship learning for helicopter control. *Communications of the ACM*, Vo. 52, No. 7, pp 97-105, 2009. DOI: 10.1145/1538788.1538812.
- [28] Ng A Y, Jin Kim H, Jordan M I, Sastry S. Autonomous helicopter flight via reinforcement learning. *Advances in Neural Information Processing Systems*, Vol. 16, pp 799-806, 2003.
- [29] Chen B M. Design and implementation of a flight control system for an unmanned rotorcraft using RPT control approach. *Asian Journal of Control*, Vol. 15, No. 1, 2013. DOI: 10.1002/asjc.504.
- [30] Kendoul F, Lara D, Fantoni-Coichot I, Lozano R. Real-time nonlinear embedded control for an autonomous quadrotor helicopter. *Journal of Guidance Control and Dynamics*, Vol. 30, No. 4, 2007. <https://doi.org/10.2514/1.27882>.
- [31] Sanchez E N, Becerra H M, Velez C M. Combining fuzzy, PID and regulation control for an autonomous mini-helicopter. *Information Sciences*, Vol. 177, No. 10, 2007. DOI: 10.1016/j.ins.2006.10.001.
- [32] Janiec T, Romicki M, Butkiewicz B. Autopilot for the unmanned helicopter – program in the Simulink environment. Institute of Aviation Scientific Publications.
- [33] Kadmiry B, Driankov D. Fuzzy control of an autonomous helicopter. *The IFSA World Congress and 20th NAFIPS International Conference*, Vancouver, Canada, 2001. DOI: 10.1109/NAFIPS.2001.943669.
- [34] Wang Q, Chen M, Xu G. Control strategy for compound coaxial helicopter trimming in steady-state flight. *The 38th European Rotorcraft Forum*, Amsterdam, Netherlands, 2012.
- [35] Bedyńska A, Bibik P, Curyło P, Czarnota N, Ceniuk M, Grabowski Ł, Łukasiewicz M. ARCHER – autonomous re-configurable compound helicopter for education and research. *The 45th European Rotorcraft Forum*, Warsaw, Poland, 2019.
- [36] Val R D, He C. FLIGHTLAB™ modeling for real-time simulation applications. *International Journal of Modeling Simulation and Scientific Computing*, Vol. 8, No. 3, 2017. DOI: 10.1142/S1793962317430036.
- [37] Topczewski S, Narkiewicz J, Bibik P. Helicopter control during landing on a moving confined platform. *IEEE Access*, Vol. 8, pp 107315–107325, 2020. DOI: 10.1109/ACCESS.2020.3000294.
- [38] Sivanandam S N, Sumathi S, Deppa S N. *Introduction to fuzzy logic using MATLAB*. 1st edition, Springer, pp 113-127, 151-155, 2007. DOI: 10.1007/978-3-540-35781-0.
- [39] Chen G, Pham T T. *Introduction to fuzzy sets, fuzzy logic and fuzzy control systems*. CRC Press LLC, pp 58-65, 2001.
- [40] Bede B. *Mathematics of fuzzy sets and fuzzy logic*. 1st edition, Springer, 2013. DOI 10.1007/978-3-642-35221-8.
- [41] Verbeke J, De Schutter J. Experimental maneuverability and agility quantification for rotary unmanned aerial vehicle. *International Journal of Micro Air Vehicles*, Vol. 10, No. 1, pp 3-11, 2017. DOI: 10.1177/1756829317736204.
- [42] United States Army Aviation and Missile Command. *Aeronautical Design Standard, Performance Specification, Handling Qualities Requirements for Military Rotorcraft*, ADS-33E-PRF, 2000.
- [43] Ivler C M, Russell K, Gong A, Berger R, Lopez M J S. Toward a UAS handling qualities specification development of UAS-specific MTEs. *Vertical Flight Society's 78th Annual Forum & Technology Display*, Ft. Worth, TX, USA, 2022.
- [44] Malinowski M. Trajectory determination based on Cubature Kalman Filter. *Autobusy: Technika, Eksploatacja, Systemy Transportowe*, Vol. 18, No. 12, pp 1114-1121, 2017.